Identification of Sunspots on SODISM Full-Disk Solar Images

Amro F. Alasta
Electrical Engineering and Computer Science)
University of Bradford
Bradford, U.K.
Amr_hard@yahoo.com
a.f.a.alasta@student.bradford.ac.uk

Abdrazag Algamudi
Electrical Engineering and Computer Science)
University of Bradford
Bradford, U.K
gamudi@yahoo.com

Rami *Qahwaji*
Electrical Engineering and Computer Science)
University of Bradford
Bradford, U.K
R.S.R.Qahwaji@bradford.ac.uk

Fatma Almesrati
Information Technology Management
University of Bradford
Bradford, U.K
enas199990@yahoo.com

ABSTRACT:

This paper presents a new method that provides the means to detect sunspots on full-disk solar images recorded by the Solar Diameter Imager and Surface Mapper (SODISM) on the PICARD satellite. The method is a totally automated detection process that achieves a sunspot recognition rate of 97.6%. The number of sunspots detected by this method strongly agrees with the NOAA catalogue. The sunspot areas calculated by this method have a 99% correlation with SOHO over the same period, and thus help to calculate the filling factor for wavelength (W.L.) 607nm.

Keywords Sunspots; SODISM; SOHO; Segmentation, PICARD, wavelength 607nm and Filling Factors.

I. INTRODUCTION

There are many satellites that observe the solar disk and detect feature activities, such as Sunspots. PICARD is one such satellite, which was launched on 15 June 2010 using the SODISM platform. Since its launch on PICARD, the SODISM telescope has recorded images every 24 hours over 7 days in the year. Level 0 (L0) data is generated every day by the PICARD Payload Data Center registered at BUSOC in Brussels. SODISM has five wavelengths, which are centered at 215.0, 393.37, 535.7, 607.1, and 782.2nm, and provide different image qualities depending on the wavelength. However, the combination of solar irradiation and instrumental contamination significantly impact on SODISM and cause degradation.[1] The W.L. 215nm channel lost more than 90% of the normalized intensity, and W.L. 393nm lost about 80% [2]; this shows a pronounced degradation in the UV channels, as illustrated in Figure 1. The degradation arises due to the polymerisation of contaminants on the front window, or on the other optical elements under the solar UV exposure. Meanwhile, the visible and near infrared channels present a temporal oscillation but remain relatively constant [1].

According to Figure 1, and with the exception of the 215nm W.L, all other wavelengths can be used to detect Sunspots. However, this paper investigates only band 607nm images, which are available at level 1B1 (level 1B data products include a number of corrections for instrument issues). In total, approximately 250 images were downloaded, from 22th September 2010 to 4th January 2014.

The format of these files was FITS, and each image has a size of 2048× 2048 pixels.

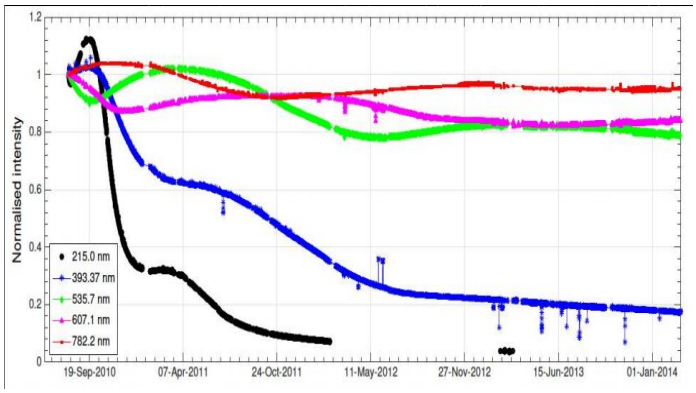

Figure 1: Normalized time series of integrated intensity of PICARD during his mission (Meftah et al. 2015).

The application of automated detection of solar features is a technique that provides robust, fast and accurate automated detection [3]. Many researchers use observatory images from the SOHO and SDO satellites to detect features such as sunspots, but as the images from SODISM have been relatively underused, this prompted an interest in working with the images.

This paper provides the following contributions:

- The provision of an automated method to detect Sunspots from SODISM images with verification.
- The provision of a filling factor and comparisons with SOHO images.
- A comparison with the NOAA catalogue.

This paper is organized as follows: Section 2 summarizes the literature survey; Section 3 describes the pre-processing approaches applied; Section 4 illustrates the accuracy between the NOAA and the proposed method; Section 5 provides the filling factor computations for the SODISM and SOHO results, which presents some experimental results; finally the conclusions and results are presented in Section 6.

[1] http://picard.projet.latmos.ipsl.fr/files.php

978-1-5386-4904-6/18/$31.00 ©2018 Crown

II. Literature Survey

In order to discover its solar radius and center, it is compulsory to detect the boundary limb of the solar disk before applying the segmentation features [4]. Once this has been established, the interior features can be analyzed, such as Sunspots, which are dark, sometimes irregularly shaped, local structures on the solar disk. There are three main types of approach to segmentation [4]: Boundary-based, Region-based, and Thresholding.

Of the three approaches, Thresholding is the simplest and quickest method [5]. However, the non-uniform brightness of the background solar disk make the global thresholding of the solar disk an impractical solution. Nevertheless, this can be modified and corrected by normalizing the image brightness in a pre-processing step [6]. Furthermore, some background regions of the solar disk in some images have different contrasts and could be darker than some sunspots in other regions.

Zharkov et al. [7] summarized and evaluated existing fully-automated, manual and semi-automated feature recognition techniques applied to different solar features, For example, in 2008, Curto et al. [5] provided a fully automated recognition approach to detect sunspots by using morphological operators. These recognition techniques [8] detect the boundaries between regions by looking for discontinuities in grey levels. Gauss smoothing and a Sobel gradient are applied to detect contours using operators that are sensitive to meaningful discontinuities in the intensity level. However, problems arise with most applications, which produce unsatisfactory results; to counter this, post-processing operations are applied.

The previous methods applied on SODISM to detect sunspots can be summarized by the following studies:

Ashmeri et al. introduced internal work[2] [9], which is a method for detecting sunspots from SODISM images (at a 535nm band). They first applied a Wavelet Harr filter to remove noise from the image, and then used a bandpass filter to remove limb darkening. Finally, Gaussian smoothing was applied to remove isolated noisy pixels. Their results were excellent and the correlation coefficient between SOHO and SODISM images was found to be 0.98.

In comparison, in 2016 Meftah et al. [10] applied a similar method to Corto et al. on SODISM 393nm data to detect sunspots and bright features. The steps of their method are as follows, and produce results that reflect the same accuracy as manual thresholding:

- Firstly, apply preprocessing on L1 SODISM data in order to obtain SODISM images with a full contrast. To reduce noise, a Median filter is applied.
- Secondly, morphological processing is applied, consisting of a top-hat operation for Sunspot detection.
- Thirdly, the Otsu threshold for the segmentation of sunspots is applied.

For the detection of bright regions, morphological processing is performed, which consists of a bottom-hat (complementing the top-hat) operation. However, if the number of detected faculae is not coherent, an iterative procedure is launched; this starts from a reduced threshold and/or increases gradually until the number of detected faculae corresponds to a fixed interval. The main disadvantage of this method is the time it requires.

In 2017, Alasta et al.[4] applied SODISM data to a 535nm W.L., and their methods were as follows:

- Firstly, determine the solar disk and record its radius and centre information.
- Secondly, convert the image scale from a signed 32 bit, to an unsigned 8 bit.
- Thirdly, use Kuwahara and À Trous filters to remove noise and other unwanted features.
- Correct any pixels that are brightness outliers, and apply a Band pass filter to display the sunspots on a normalized background.
- Finally, apply a Threshold to obtain a mask image and determine the sunspot locations.

The results of this method compared with the SOHO filling factor and the correlation coefficient between the two data sets is 98.5%.

III. Pre- processing and features detection

The preview method for detecting sunspots has limitations, because a manual threshold has to be entered. Moreover, these steps are the most time consuming, and the method only applies to 393nm W.L. images, so does not apply to large data.

The method for this study overcomes problems associated with time consumption because it is automated and can be applied on large data for 607nm W.L. It also provides better results than those produced on a 535nm W.L. The method is developed to automatically detect sunspots in 607nm SODISM L1 images and is programmed into MATLAB; it adopts the following steps, shown as Algorithms 1 and 2:

Algorithm 1: Extraction of the solar limb

[i] Obtain a clean solar disk without noise and sunspots; this can be achieved by applying a dilation and then an erosion operation, i.e. a closing operation with a structuring element (SE) on an original SODISM image

[ii] Choose a circular SE of 30 pixels radius (this value was chosen by cross validation). The sample result is shown in Figure 2.b

[iii] To secure the solar limb, determine the border edges; thus, shrink the solar disk by one pixel (filtered image in Figure 1.b) to produce a smaller image,

[iv] Then subtract the new image from the filtered image; the result is illustrated in Figure 2.c

[v] Eliminate CCD noises by utilizing a Kuwahara Filter (refer to Figures 2.d and 2.e)

[vi] Apply a binary overlay plugin between the original and solar limb images; it is labeled with a red colour and overlapped on the original image, as shown in Figure 2.f.

[2] https://projects.pmodwrc.ch/solid/index.php/links/10-news-archive/31-deliverables

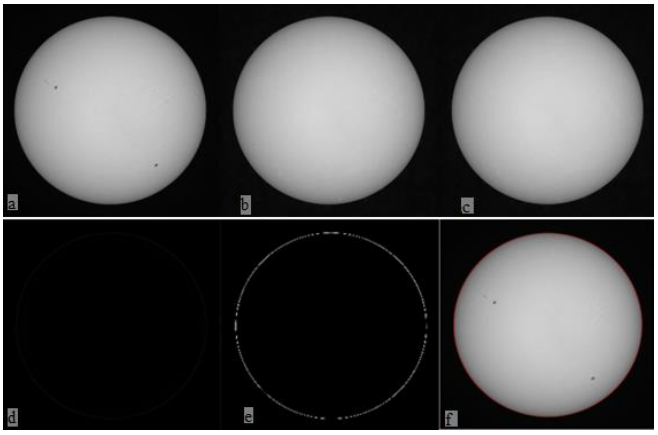

Figure 2: (as shown from left to right, top to bottom): (a) the original image; (b) the filtered image; (c) the shrunken image of the solar disk, where the radius is 1 pixel smaller than that in (b); (d) the solar limb shown in a grey image; (e) solar limbs; (f) red colour around disk shows the solar limb label.

IV. DETECTION OF SUNSPOTS AND VERIFICATION

This involves the recognition of sunspots on the solar disk after the solar limb has been extracted. Due to the limited resolution of the data, the sunspot umbra and penumbra are not separated in the SODISM images; rather they are considered and processed as a whole The steps outlined in Algorithm 2 enable the identification of sunspots (refer to Figure 3 for the associated images).

Algorithm 2: The Detection of Sunspots

[i] Process the original image from the PICARD website using the proposed quality enhancement method; the sample output is shown in Figure 3.a

[ii] Compute the gradient of the sunspot boundaries (refer to Figure 3.a)

[iii] Fill the holes with a closing operation; this leads to the removal of dark regions surrounded by bright crests in grayscale images

[iv] Compute the image obtained in 3.a and the gradient image obtained in [ii] (i.e. the difference between Figures 3.a and 3.b will yield 3.c).

[v] Separate the sunspot gradient from the noises, as shown in Figure 3.c, This operation lies the threshold of the darkness of Figure 3.c, Many experiments were applied to ascertain a suitable value and an intensity of 15% (in Figure 3.c) was identified; however, due to the solar limb darkening, it was noted that the sunspot's gradient was lower at the solar limb, so the threshold was 10% in the region of the solar disk.

[vi] Remove the unwanted noises using the Kuwahara Filter. Employ the Extended Min and Max operation as a marker detection to enable segmentation, Figure 3.d shows the sunspot candidate.

[vii] Acquire sunspots from the candidates, as shown in Figure 3.d. This study considered the candidates as verified sunspots in which the difference between the maximum and minimum grey values of a pixel are bigger than 5, and the other regions are ignored.

[viii] Apply a binary overlay in a red color and superimpose the original image, (Figure 4 shows the sample result).

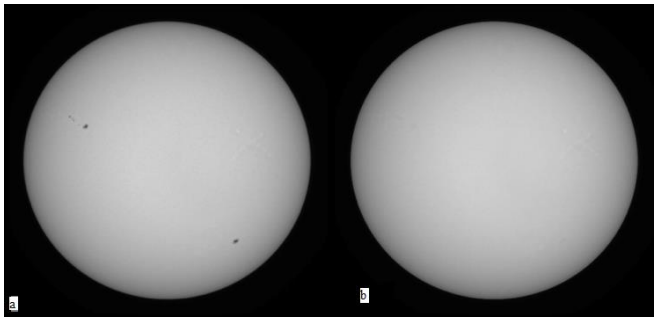

Figure 3: (a) The original image disturbed by instrument noises; (b) the filtered image without sunspots

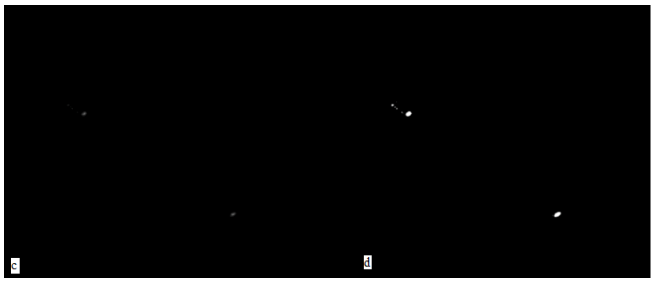

Figure 3c: (c) the gradient on the image; (d) the binary image showing sunspot candidates

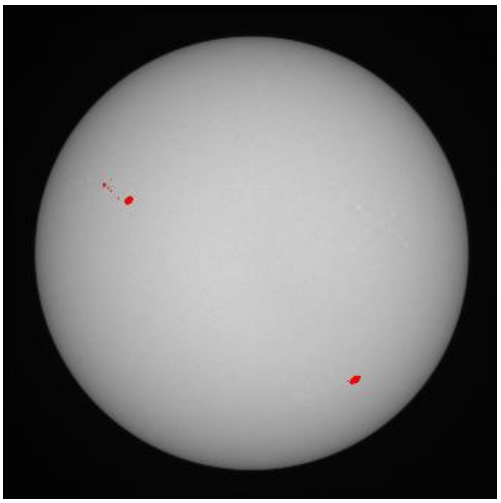

Figure 4: The recognised and superimposed sunspots on the original image

V. ACCURACY OF THE AUTOMATIC PROCEDURE COMPARED WITH THE NOAA CATALOGUE

The data from the 607nm W.L. from August and September 2010, for both the automated and NOAA are illustrated in Table 1. The table has five columns: the first shows the date on which the image was captured; the second represents the number of sunspots in the image (manually counted), and the third column shows the number of sunspots detected by the study's automatic pipeline. The fourth

column shows the false rejection rate (FRR), i.e. the number of sunspots detected automatically, but not by the NOAA catalogue, and finally, the last column is false acceptance rate (FAR) i.e. the number of sunspots detected by the NOAA catalogue but not by the automatic method. The rationale for computing the FRR and FAR is to evaluate the proposed pipeline in accordance with the approaches of past research [8]. SOHO images have been used as reference in order to overcome small sunspots that were missed through manual processing because of the limitation of visible conditions. The total number of sunspots detected is listed in the last row of the table for both the automated method and the NOAA respectively. The recognition rate calculated as follows:

$$= \frac{sum\ of\ the\ automatic\ method\ -\ sum\ of\ the\ FAR}{sum\ of\ NOAA}$$

$$\frac{89\ -\ 7}{84} \times 100 = 97.6\%$$

Table 1: The Comparison Of Sunspot Detected By The Automatic Procedure With NOAA One.

Date	SSs No. (automatic method)	Time of SSs in SODISM image	SSs No. (NOAA catalogue)	FRR	FAR
05/08/2010	4	04:49	4	0	0
06/08/2010	4	01:07	4	0	0
07/08/2010	4	01:07	4	0	0
09/08/2010	4	05:27	4	0	0
10/08/2010	4	01:17	3	1	0
11/08/2010	5	05:43	5	0	0
12/08/2010	4	00:47	0	4	0
13/08/2010	4	04:01	2	2	0
14/08/2010	2	05:27	2	0	0
15/08/2010	2	00:31	2	0	0
16/08/2010	3	03:21	3	0	0
17/08/2010	2	05:39	2	0	0
18/08/2010	1	01:25	2	0	1
19/08/2010	1	01:33	2	0	1
20/08/2010	0	03:15	1	0	1
21/08/2010	0	03:59	0	0	0
22/08/2010	0	00:07	0	0	0
23/08/2010	0	02:21	0	0	0
24/08/2010	0	05:41	1	0	1
25/08/2010	1	00:51	0	1	0
26/08/2010	2	06:39	2	0	0
27/08/2010	1	01:55	1	0	0
28/08/2010	1	05:47	1	0	0
29/08/2010	2	01:11	2	0	0
30/08/2010	2	02:51	2	0	0
04/09/2010	3	12:13	3	0	0
05/09/2010	4	06:19	4	0	0
06/09/2010	2	02:07	1	1	0
07/09/2010	0	21:20	1	0	1
11/09/2010	0	00:12	0	0	0
12/09/2010	1	08:05	2	0	1
13/09/2010	3	00:13	1	2	0
20/09/2010	3	07:59	2	1	0
22/09/2010	2	04:49	2	0	0
23/09/2010	2	14:11	2	0	0
24/09/2010	2	03:15	2	0	0
25/09/2010	2	03:25	2	0	0
26/09/2010	2	03:25	3	0	1
27/09/2010	3	03:27	3	0	0
29/09/2010	3	04:21	3	0	0
30/09/2010	4	00:47	4	0	0
Total	**89**		**84**	**12**	**7**

VI. FILLING FACTORS COMPUTATION

The filling factor is calculated as a function of the radial position on the sun disk. Thus, the calculated filling factors for a particular feature reflect the fraction of the solar disk covered by the feature, to which a synthetic spectra reference is assigned.[11] Eleven concentric rings divide the solar disk; these start with an inner radius (RI), and conclude with an outer radius (RO). Figure 5 shows filling factor coverage for sunspots.

The data obtained for the 607nm W.L. were collected from 22th September 2010 until 1st January 2014. The filling factor of this data sharing with SOHO have been calculated and compared with SODISM over the same period (i.e. September, October November and December 2010). The correlation coefficient was 99%, which reflects that the method gives excellent results for the 607nm W.L. Figure 6 shows the comparison with the SOHO satellite

Table 2: Relative radius values

Index	Inner radius (relative radius)	Outer radius (relative radius)
1	0.00	0.07
2	0.07	0.16
3	0.16	0.25
4	0.25	0.35
5	0.35	0.45
6	0.45	0.55
7	0.55	0.65
8	0.65	0.75
9	0.75	0.85
10	0.85	0.95
11	0.95	1.05

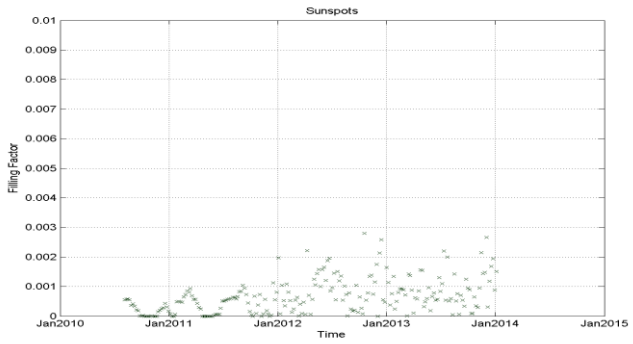

Figure 5: The filling factors (area coverage) for sunspots

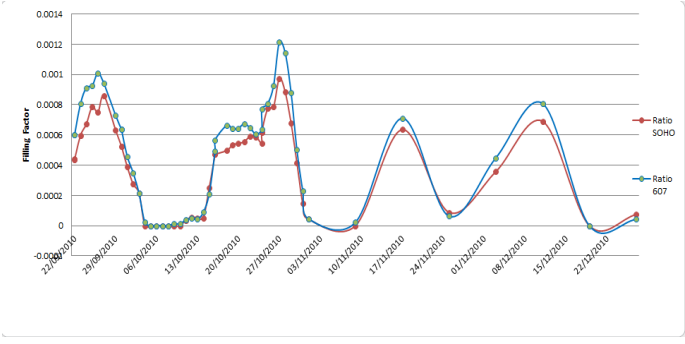

Figure 6: Filling factor calculation of sunspot from SOHO and SODISM images from 22th September 2010 until 25 December 2010

VII. Conclusions and results

The proposed segmentation method has been applied to the entire downloaded 607nm image data in order to detect sunspots and calculate their filling factors. Moreover, a comparison with the NOAA catalogue has been conducted. Figure 5 shows filling factor coverage from October 2010 until the end of life for the Picard satellite, which was on 1st January 2014. Moreover, Figure 6 shows a comparison between the filling factors calculated for the SODISM 607nm images and the MDI intensitygram images from the SOHO satellite over a similar period (i.e. from September, 22th 2010 to December 24th, 2010). The comparison between the two values, or measure of dependence between the two quantities, is calculated as Pearson's correlation coefficient, which is 99% between SOHO and SODISM. Moreover, from Table 1, the recognition rate for the proposed method is approximately 98%.

It is possible to use suitable automated methods for detecting sunspots on SODISM images, despite the image degradation throughout the lifetime of PICARD. The biggest advantage is the reduction in time consumption. There are only a few methods applied to segmented SODISM images; the first was by Meftah et al. [11], which was applied to 393nm W.L. but needed manual interaction to optimize the threshold, which was calculated using the Otsu method [7]. The second method was developed in the internal work by Ahmed et al., and shows both good results and a correlation coefficient of 98% [9] between the SODISM and SOHO images. This was only slightly less than that achieved in the same period in the third method by Alasta et al., which successfully detected sunspots on 535nm W.L. images over the lifetime of PICARD, and then calculated the filling factors, Furthermore, a comparison of sunspots filling factors between SOHO and SODISM images shows an excellent match over the early period when they are both available, and achieve a correlation coefficient of 98.5% [4].
This method was applied to the W.L. 607nm; it is completely automated, which makes it easy to apply to very large data images. The correlation coefficient is 0.99, which reflects excellent results. The results in Figure 6 show that the filling factors for SODISM and SOHO are slightly different in amplitude despite mostly changing instep. This is most evident between 22 September 2010 and 29 September 2010 when there is a somewhat lower correlation coefficient ($\approx$0.95). Nevertheless, this is still better than the results from the previous method at a 535nm W.L. over the same period, which shows a correlation 0.92. This could be related to the fact that the SOHO data corresponds to a different wavelength (676.8nm) than the SODISM images. However, this is the first automated method to achieve 0.99 corrections between SOHO and SODISM. Table 2 illustrates a key technique for identifying regions of interest; image segmentation was also explored, investigated and deployed. Similarly, a thorough evaluation and comparison of the results from similar works was conducted. In general, the system developed and described in this paper has proven to be promising, in that, out of 89 sunspots, it automatically detected around 98%, which is comparable with the NOAA catalogue of sunspots

References

[1] M. Meftah, a Hauchecorne, T. Corbard, E. Bertran, M. Chaigneau, and M. Meissonnier, "PICARD SODISM, a space telescope to study the Sun from the middle ultraviolet to the near infrared," no. January, pp. 1–38, 2014.

[2] [2] M. Meftah, A. Irbah, A. Hauchecorne, and J.-F. Hochedez, "PICARD payload thermal control system and general impact of the space environment on astronomical observations," no. May 2013, p. 87390B, 2013.

[3] [3] R. Qahwaji and T. Colak, "Automatic detection and verification of solar features," Int. J. Imaging Syst. Technol., vol. 15, pp. 199–210, 2005.

[4] [4] A. F. Alasta, A. Algamudi, R. Qahwaji, S. Ipson, and T. A. Nagern, "Automatic sunspots detection on SODISM solar images," in 2017 Seventh International Conference on Innovative Computing Technology (INTECH), 2017, pp. 115–119.

[5] [5] J. J. Curto, M. Blanca, and E. Martínez, "Automatic sunspots detection on full-disk solar images using mathematical morphology," Sol. Phys., vol. 250, no. 2, pp. 411–429, 2008.

[6] [6] S. Zhang, H. Yang, and L. Singh, "Increased information leakage from text," CEUR Workshop Proc., vol. 1225, no. 2003, pp. 41–42, 2014.

[7] [7] S. Zharkov, V. Zharkova, S. Ipson, and A. Benkhalil, "Technique for automated recognition of sunspots on full-disk solar images," EURASIP J. Appl. Signal Processing, vol. 2005, no. 15, pp. 2573–2584, 2005.

[8] [8] V. Zharkova, S. Ipson, A. Benkhalil, and S. Zharkov, "Feature recognition in solar images," Artif. Intell. Rev., vol. 23, no. 3, pp. 209–266, 2005.

[9] [9] O. Ahmed. Rami Qahwaji, Stan Ipson, "SOLID D3.5 Filling factors catalogue for PICARD images SOLID," First Eur. Compr. Sol. Irradiance Data Exploit., pp. 1–8, 2015.

[10] [10] M. Meftah, T. Corbard, A. Hauchecorne, A. Irbah, P. Boumier, A. Chevalier, W. Schmutz, R. Ikhlef, F. Morand, C. Renaud, J.-F. Hochedez, G. Cessateur, S. Turck-Chièze, D. Salabert, M. Rouzé, M. van Ruymbeke, P. Zhu, S. Kholikov, S. Koller, C. Conscience, S. Dewitte, L. Damé, and D. Djafer, "Main results of the PICARD mission," no. July, p. 99040Z, 2016.

[11] [11] O. Ashamari, R. Qahwaji, S. Ipson, M. Schöll, O. Nibouche, and M. Haberreiter, "Identification of photospheric activity features from SOHO/MDI data using the ASAP tool," J. Sp. Weather Sp. Clim., vol. 5, p. A15, 2015.